INSTITUTE OF PHYSICS PUBLISHING INVERSE PROBLEMS

Inverse Problems **18** (2002) 221–235 PII: S0266-5611(02)26430-8

Synthetic aperture inversion

Clifford J Nolan and Margaret Cheney[1]

Department of Mathematical Sciences, Rensselaer Polytechnic Institute, Troy, NY 12180, USA

E-mail: clifford.nolan@ul.ie and cheney@rpi.edu

Received 29 June 2001, in final form 8 October 2001
Published 15 January 2002
Online at stacks.iop.org/IP/18/221

Abstract

This paper considers synthetic aperture radar and other synthetic aperture imaging systems in which a backscattered wave is measured from a variety of locations.

The paper begins with a (linearized) mathematical model, based on the wave equation, that includes the effects of limited bandwidth and the antenna beam pattern. The model includes antennas with poor directionality, such as are needed in the problem of foliage-penetrating radar, and can also accommodate other effects such as antenna motion and steering.

For this mathematical model, we use the tools of microlocal analysis to develop and analyse a three-dimensional imaging algorithm that applies to measurements made on a two-dimensional surface. The analysis shows that simple backprojection should result in an image of the singularities in the scattering region. This image can be improved by following the backprojection with a spatially variable filter that includes not only the antenna beam pattern and source waveform but also a certain geometrical scaling factor called the Beylkin determinant. Moreover, we show how to combine the backprojection and filtering in one step. The resulting algorithm places singularities in the correct locations, with the correct orientations and strengths.

The algorithm is analysed to determine which information about the scattering region is reconstructed and to determine the resolution. We introduce a notion of directional resolution to treat the reconstruction of walls and other directional elements. We also determine the fineness with which the data must be sampled in order for the theoretical analysis to apply. Finally, we relate the present analysis to previous work and discuss briefly implications for the case of a single flight track.

[1] Corresponding address: Mathematical Sciences, Research Institute, 1000 Centennial Drive, #5070, Berkeley, CA 94720-5070, USA. After 14 December 2001, Contact at: Math Sciences, Amos Eaton Hall, RPI, 110 8th Street Troy, NY 12180, USA.

1. Introduction

In synthetic aperture radar (SAR) imaging [7, 8, 10, 14, 15, 17], a plane or satellite carrying an antenna moves along a flight track. The antenna emits pulses of electromagnetic radiation, which scatter off the terrain, and the scattered waves are detected with the same antenna. The received signals are then used to produce an image of the terrain (see figure 1).

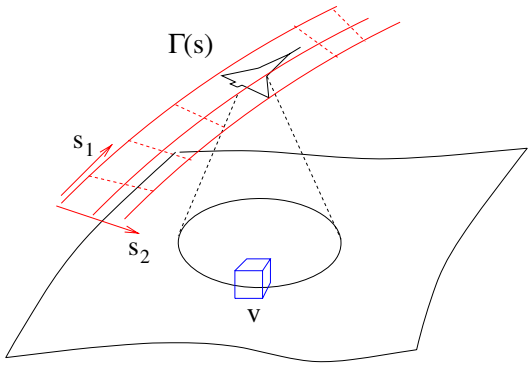

Figure 1. Acquisition geometry for three-dimensional SAR.

A similar procedure is used for synthetic aperture sonar, using an array of transducers instead of an antenna; here the goal is to map the seafloor. Synthetic aperture focusing techniques are also used in non-destructive evaluation [19, 24]. The techniques employed in this paper are closely related to those used in the geophysics community [3, 4, 6, 27, 29].

Work has been done on the reconstruction problem for the case of a perfect point source moving along a single straight flight track, under the assumption that measurements are made for all times at each flight-track position. For this case, an exact inversion formula was given in [1, 16, 22] and a fast algorithm in [26].

We consider the case in which multiple passes are made over the same scene, so that backscattering measurements are made for positions that sample a two-dimensional surface of sensor positions. The data depend on three variables, namely time and position on the measurement surface, so we expect to be able to reconstruct a function of three variables. In particular, we expect to be able to make a three-dimensional reconstruction of the region under a forest canopy, including the bare-earth topography.

We use the methods of microlocal analysis [11, 20, 21, 34], which enable us to reconstruct the singularities in the scattering region [3, 4, 6, 25, 29, 31]. Singularities correspond to edges and boundaries between different materials, so an image of the singularities gives us an image of structures such as walls and vehicles. The microlocal methods give us reconstruction formulae even in the case when the data are incomplete and non-ideal. In particular, these methods can accommodate the varying antenna beam patterns that arise in the cases of non-ideal antenna motion and gain, and with appropriate adjustments the same reconstruction formulae apply to both spotlight-mode [9] and stripmap-mode SAR [15, 17]. In addition, the methods allow us to deal with data that is limited in time and space. Microlocal reconstruction techniques have been used to advantage in the geophysics community, where they have been found to be fast and robust [4, 6].

Microlocal methods have the limitation that they can only be expected to provide a reconstruction of singularities and their strengths. However, in practice they often reduce to the exact inversion formulae that are known for idealized cases. As we see in section 7.1, this is the case for the formulae we develop in this paper.

The problem of imaging singularities from backscattered data was also considered by Louis and Quinto [25] in their study of the spherical Radon transform. They showed that singularities in the transform data determine the location and direction of certain singularities in the scattering region. Our work differs from theirs in that we consider the practical case of non-ideal antenna beam patterns, and in that we give an explicit reconstruction algorithm.

We first give an algorithm for locating the singularities in the scattering region. We show how this process can be followed by a spatially varying filter to provide accurate strengths of singularities. In particular, we show how to correct for the antenna beam pattern, which may vary with position on the measurement surface. Moreover, we show that these two operations can be combined into one. We explain exactly which features are reconstructed. We then analyse the resolution of the algorithm, introducing a notion of directional resolution in addition to using more conventional measures of resolution. We consider also the issue of how finely the data must be sampled in order for the theoretical analysis to apply. Finally, we discuss implications of our analysis for the single flight-track case and show how it relates to previous work.

In the paper we discuss explicitly the radar case, but the analysis applies equally well to sonar and ultrasound imaging.

2. The mathematical model

2.1. A model for the wave propagation

For SAR, the correct model is of course Maxwell's equations, but the simpler scalar wave equation is commonly used:

$$\left(\nabla^2 - \frac{1}{c^2(x)}\partial_t^2\right) U(t,x) = 0, \tag{1}$$

where the function c is the wave propagation speed. Each component of the electric and magnetic fields in free space satisfies (1); thus it is a good model for the propagation of electromagnetic waves in dry air.

For sonar and ultrasound, (1) is a good model. For geophysics it is sometimes used but the equations of linear elasticity are more appropriate.

We assume

Assumption 1. The volume to be imaged is well separated from the region where the sensors are located, and that in the intervening region, $c(x) = c_0$.

For radar applications, c_0 is the speed of light in vacuum.

2.2. A model for the field from an antenna

In free space, the field G_0 at (t, x) due to a delta function point source at the origin at time 0 is given by [33]

$$G_0(t,x) = \frac{\delta(t - |x|/c_0)}{4\pi|x|}, \tag{2}$$

which satisfies

$$(\nabla^2 - c_0^{-2}\partial_t^2)G_0(t,x) = -\delta(t)\delta(x).$$

The antenna, however, is not a point source [41] $\delta(x)$, and the signal sent to the antenna is not a delta function $\delta(t)$. Therefore we replace $\delta(x)$ by $J_s(x)$ and $\delta(t)$ by the waveform $P(t)$. In the radar case, J_s is the time derivative of the current distribution over the antenna,

and $P(t)$ is the waveform sent to the antenna. The waveform $P(t)$ can be of almost any shape, but commonly a *chirp* of the form $P(t) = \mathrm{rect}(t)\exp(\mathrm{i}\alpha t^2)$ is used. Examples of commonly used antennas include rectangular arrays [12, 13, 42], horns [32] and dipoles [32].

The field emanating from the antenna then satisfies

$$(\nabla^2 - c_0^{-2}\partial_t^2)U^{in}(t,x) = -P(t)J_s(x) \tag{3}$$

so that

$$\begin{aligned} U^{in}(t,x) &= G_0 * (PJ) \\ &= \int \frac{P(t-|x-y|/c_0)}{4\pi|x-y|} J_s(y)\,\mathrm{d}y \end{aligned} \tag{4}$$

where the star denotes convolution in t and x.

We write P in terms of its Fourier transform p:

$$P(t) = \int \mathrm{e}^{-\mathrm{i}\omega t} p(\omega)\,\mathrm{d}\omega. \tag{5}$$

In practice, the waveform P is such that only a certain union of intervals $[-\omega_{\max}, -\omega_{\min}] \cup [\omega_{\min}, \omega_{\max}]$ contributes significantly to (5); we call this set the *effective support* of $p(\omega)$ (eff. supp (p)). The difference $(\omega_{\max} - \omega_{\min})$ is the (angular-frequency) *bandwidth*. We assume that $\omega_{\min}$ is greater than zero. The fact that P is band limited means that ultimately we reconstruct band-limited approximations to singularities rather than the actual singularities.

With the notation (5), (4) becomes

$$U^{in}(t,x) = \int \frac{\mathrm{e}^{-\mathrm{i}\omega(t-|x-y|/c_0)}}{4\pi|x-y|} p(\omega)J_s(y)\,\mathrm{d}\omega\,\mathrm{d}y. \tag{6}$$

Next we assume that the antenna (or sensor array) is small compared with the distance to the scatterers. We denote the centre of the antenna by y^0; thus a point on the antenna can be written $y = y^0 + q$, where q is a vector from the centre of the antenna to a point on the antenna. In this notation, the assumption that the scattering location x is far from the antenna can be expressed $|q| \ll |x - y^0|$. For such x, we can write

$$|x-y| = |x-y^0| - (\widehat{x-y^0})\cdot q + \mathrm{O}(|q|^2/|x-y^0|), \tag{7}$$

where $\hat{y}$ denotes a unit vector in the same direction as y.

We use the expansion (7) in (6) to obtain

$$\begin{aligned} U^{in}(t,x) &\approx \int \frac{\mathrm{e}^{-\mathrm{i}\omega(t-|x-y^0|/c_0)}}{4\pi|x-y^0|} \mathrm{e}^{-\mathrm{i}\omega(\widehat{x-y^0})\cdot q} p(\omega)J_s(y^0+q)\,\mathrm{d}\omega\,\mathrm{d}q \\ &\approx \int \frac{\mathrm{e}^{-\mathrm{i}\omega(t-|x-y^0|/c_0)}}{4\pi|x-y^0|} p(\omega) j_s(\omega(\widehat{x-y^0}), y^0)\,\mathrm{d}\omega \end{aligned} \tag{8}$$

where we have written

$$\begin{aligned} j_s(\omega(\widehat{x-y^0}), y^0) &= \int \mathrm{e}^{-\mathrm{i}\omega(\widehat{x-y^0})\cdot q} J_s(y^0+q)\,\mathrm{d}q \\ &= \mathrm{e}^{\mathrm{i}\omega(\widehat{x-y^0})\cdot y^0} \int \mathrm{e}^{-\mathrm{i}\omega(\widehat{x-y^0})\cdot v} J_s(v)\,\mathrm{d}v. \end{aligned} \tag{9}$$

This Fourier transform of the current density gives the antenna beam pattern in the far-field at each fixed frequency. Generally the antenna beam pattern is nearly independent of frequency over the effective support of $p(\omega)$; indeed, a great deal of work goes into designing antennas for which this is the case. Antennas whose beam patterns are nearly constant over a wide frequency band are called *broadband* antennas.

We see from (8) that the field emanating from the antenna is a superposition of fixed-frequency point sources that are each shaped by the antenna beam pattern. The field (8) clearly depends on y^0, the location of the centre of the antenna; consequently we write $U^{in}_{y^0}$ to indicate this dependence.

2.3. A linearized scattering model

Since we are ignoring polarization, the current density J_s is scalar and the model we use for wave propagation including the source is

$$(\nabla^2 - c^{-2}(x)\partial_t^2)U(t,x) = -P(t)J_s(x). \tag{10}$$

We write $U = U^{in} + U^{sc}$ in (10) and use (3) to obtain

$$(\nabla^2 - c_0^{-2}\partial_t^2)U^{sc}(t,x) = -V(x)\partial_t^2 U(t,x), \tag{11}$$

where

$$V(x) = \frac{1}{c_0^2} - \frac{1}{c^2(x)}. \tag{12}$$

The *reflectivity function* V contains all the information about how the medium differs from free space. It is V, or at least its discontinuities and other singularities, that we want to recover.

We can write (11) as an integral equation

$$U^{sc}(t,x) = \int G_0(t-\tau, x-z)V(z)\partial_\tau^2 U(\tau,z)\,\mathrm{d}\tau\,\mathrm{d}z. \tag{13}$$

A commonly used approximation [19, 24], often called the *Born approximation* or the *single scattering approximation*, is to replace the full field U on the right side of (13) and (11) by the incident field U^{in}, which converts (13) to

$$\begin{aligned} U^{sc}(t,x) &\approx \int G_0(t-\tau, x-z)V(z)\partial_\tau^2 U^{in}(\tau,z)\,\mathrm{d}\tau\,\mathrm{d}z \\ &= \int \frac{V(z)}{4\pi|x-z|}\partial_t^2 U^{in}(t-|x-z|/c_0, z)\,\mathrm{d}z. \end{aligned} \tag{14}$$

The value of this approximation is that it removes the nonlinearity in the inverse problem: it replaces the product of two unknowns (V and U) by a single unknown (V) multiplied by the known incident field.

The Born approximation makes the problem simpler, but it is not necessarily a good approximation. Another linearizing approximation that can be used for reflection from smooth surfaces is the *Kirchhoff approximation*, in which the scattered field is replaced by its geometrical optics approximation [6, 24]. Here, however, we consider only the Born approximation.

For the incident field (8), (14) becomes

$$U^{sc}_{y^0}(t,x) \approx \int \frac{\mathrm{e}^{-\mathrm{i}\omega((t-(|x-z|+|z-y^0|)/c_0)}}{(4\pi)^2|x-z||z-y^0|}\omega^2 p(\omega) j_s(\omega\widehat{(z-y^0)}, y^0)V(z)\,\mathrm{d}\omega\,\mathrm{d}z. \tag{15}$$

At the centre $x = y_0$ of the antenna,

$$U^{sc}_{y^0}(t,y^0) \approx \int \frac{\mathrm{e}^{-\mathrm{i}\omega(t-2|z-y^0|/c_0)}}{(4\pi)^2|z-y^0|^2}\omega^2 p(\omega) j_s(\omega\widehat{(z-y^0)}, y^0)V(z)\,\mathrm{d}\omega\,\mathrm{d}z. \tag{16}$$

In practice, the field is measured not at the centre of the antenna but is integrated over the whole antenna. The resulting signal can be calculated with the help of (7) and involves a beam pattern

for reception $j_r(\omega(\widehat{z-y^0}), y^0)$. (Normally, when the same antenna is used for transmission and reception, $j_r = j_s$.) Thus an expression for the signal measured at antenna location y is

$$S(t,y) = \int_{\text{antenna}} U_y^{sc}(t,x)\,\mathrm{d}x$$
$$\approx \int \frac{\mathrm{e}^{-\mathrm{i}\omega(t-2|z-y|/c_0)}}{(4\pi)^2|z-y|^2}\omega^2 p(\omega) j_s(\omega(\widehat{z-y}), y) j_r(\omega(\widehat{z-y}), y) V(z)\,\mathrm{d}\omega\,\mathrm{d}z. \tag{17}$$

The idealized inverse problem is to determine V from knowledge of S for all t and for y on a surface. This surface we parametrize by $\{\Gamma(s) : s = (s_1, s_2)$, where $s_1^{\min} < s_1 < s_1^{\max}$, $s_2^{\min} < s_2 < s_2^{\max}\}$. The abrupt edges of this surface tend to cause artefacts in the image [30]; consequently it is useful to multiply the data by a smooth taper function or *mute*[2] $m(s,t)$ supported in $(s,t) \in [s_1^{\min}, s_1^{\max}] \times [s_2^{\min}, s_2^{\max}] \times [0,T]$.

We denote the map from scene V to data $d = mS$ by F, where

$$FV(s,t) = \int \mathrm{e}^{-\mathrm{i}\omega(t-2|x-\Gamma(s)|/c_0)} A(x,s,t,\omega) V(x)\,\mathrm{d}\omega\,\mathrm{d}x, \tag{18}$$

where

$$A(x,s,t,\omega) = \frac{\omega^2 p(\omega) j_s(\omega(\widehat{x-\Gamma(s)}), \Gamma(s)) j_r(\omega(\widehat{x-\Gamma(s)}), \Gamma(s)) m(s,t)}{(4\pi)^2|x-\Gamma(s)|^2}. \tag{19}$$

In practice, the measured signal is subject to a variety of other effects, such as antenna motion and steering; these effects can be included through the s-dependence of the antenna beam pattern.

We assume

Assumption 2. The amplitude A of (18) satisfies

$$\sup_{(s,t,x)\in K} |\partial_\omega^\alpha \partial_s^\beta \partial_t^\delta \partial_x^\rho A(x,s,t,\omega)| \leqslant C_{K,\alpha,\beta,\delta,\rho}(1+\omega^2)^{(2-|\alpha|)/2} \tag{20}$$

where K is any compact set and $\rho = (\rho_1, \rho_2)$.

This assumption is valid for example when the source waveform P is approximately a delta function and the antenna is sufficiently broadband. Under this assumption, the 'forward' operator F is an example of a Fourier integral operator (FIO) [11, 20, 34].

3. Formation of the image

Our goal is to reconstruct an image of the scatterers. We do this first in two steps: first we translate singularities in the data to singularities in the scattering region (migration), and then we correct the amplitudes. Later, we combine these steps into one.

Singularities in the scattering region correspond to boundaries between different materials. These singularities can have both a location and a direction. For example, locally a smooth wall perpendicular to the direction $\hat{v}$ might be modelled by a reflectivity function of the form

$$V(x) = \delta(x \cdot \hat{v}) = (2\pi)^{-1} \int \mathrm{e}^{\mathrm{i}x\cdot\hat{v}\rho}\mathrm{d}\rho. \tag{21}$$

Such a reflectivity function has a singularity in the direction $\hat{v}$; this can be seen from the fact that the Fourier transform of (21) does not decay rapidly in direction $\hat{v}$. In our image, we would like to have the wall located at the correct position with the correct orientation $\hat{v}$.

A small scatterer could be modelled by a delta function $V(x) = \delta(x)$, which is a superposition of (21) over all directions. Such a point scatterer has singularities in all directions; this corresponds to the lack of decay of its Fourier transform in all directions.

[2] Geophysics terminology.

3.1. Migration/backprojection/matched filtering

In the first step, we apply an operator that reconstructs the locations of the singularities of the scattering region. Putting the singularities in the correct locations can be done with a *matched filter*[3] [35], which is also called a *backprojection*[4] or *migration*[5] operator

$$I(z) := (Md)(z) = \int e^{i\omega(t-2|z-\Gamma(s)|/c_0)} d(s,t)\, d\omega\, ds\, dt. \tag{22}$$

The key property of M is that it has the same phase as the adjoint F^*. We show in the appendix that applying the matched filter M to the data is a legal operation in the case of distributions.

The following calculation shows that this matched filter puts the singularities in the correct locations. Using $d = FV$ in (22) results in

$$MFV(z) = \int e^{i\omega(t-2|z-\Gamma(s)|/c_0)} e^{-i\tilde{\omega}(t-2|x-\Gamma(s)|/c_0)} A(x,s,t,\tilde{\omega}) V(x)\, d\tilde{\omega}\, d\omega\, dx\, ds\, dt. \tag{23}$$

In (23), we make the change of variables $\tilde{\omega} = \omega u$. The t and u integrals of (23) are then

$$\omega \int e^{i\omega(t-ut+2u|x-\Gamma(s)|/c_0)} A(x,s,t,\omega u)\, du\, dt. \tag{24}$$

Next we use the method of stationary phase, which states [5, 20, 21].

Theorem 3.1. *If a is a smooth function of compact support on $\boldsymbol{R}^n$, and ϕ has only non-degenerate critical points, then as $\omega \to \infty$,*

$$\int e^{i\omega\phi(x)} a(x)\, dx = \sum_{\{x^0 : D\phi(x^0)=0\}} \left(\frac{2\pi}{\omega}\right)^{n/2} e^{i\omega\phi(x^0)} a(x^0) \frac{e^{i\pi \operatorname{sgn} D^2\phi(x^0)/4}}{\sqrt{|\det(D^2\phi(x^0))|}} + O(\omega^{-(n-2)/2}). \tag{25}$$

Here $D\phi$ denotes the gradient of ϕ, $D^2\phi$ denotes the Hessian of ϕ, and sgn *is the signature.*

In (24) we perform a large-ω stationary phase calculation in the variables u and t. Repeated integration by parts in the t variable shows that away from $u = 1$, (24) decays rapidly in ω, so the leading large-ω behaviour is determined by a compact neighbourhood of $u = 1$. After substituting the stationary phase result back into (23), we obtain

$$MFV(z) = 2\pi \int e^{i2\omega(|x-\Gamma(s)|-|z-\Gamma(s)|)/c_0} A(x,s,|x-\Gamma(s)|,\omega) V(x)\, d\omega\, ds\, dx + E_1(z), \tag{26}$$

where E_1 is a function smoother than the first term on the right-hand side. In the exponent of (26), we use the integral form of the remainder for Taylor's theorem to write

$$2\omega(|x-\Gamma(s)| - |z-\Gamma(s)|)/c_0 = (z-x)\cdot \Xi(z,x,s,\omega); \tag{27}$$

explicitly, Ξ is given by

$$\Xi(z,x,s,\omega) = \frac{2\omega}{c_0} \int_0^1 \frac{\Gamma(s) - (\lambda z + (1-\lambda)x)}{|\Gamma(s) - (\lambda z + (1-\lambda)x)|}\, d\lambda; \tag{28}$$

when $z = x$, it is simply

$$\Xi(z,z,s,\omega) = (2\omega/c_0)(\widehat{\Gamma(s) - z}). \tag{29}$$

[3] Signal processing terminology.
[4] X-ray tomography terminology.
[5] Geophysics terminology.

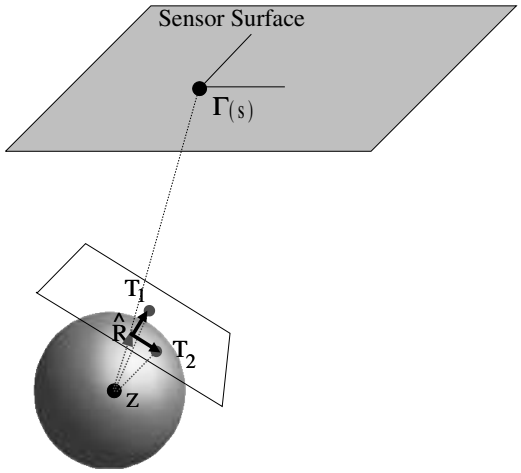

Figure 2. The vectors used to compute the Beylkin determinant.

In (26), we make the change of variables $(s, \omega) \to \xi = \Xi(z, x, s, \omega)$. This transforms the integral (26) into

$$MFV(z) = 2\pi \iint_{S_z} \mathrm{e}^{\mathrm{i}(z-x)\cdot\xi} A(x, s(\xi), |x - \Gamma(s(\xi))|, \omega(\xi)) \times \left|\frac{\partial(s,\omega)}{\partial\xi}\right| (z, x, s(\xi), \omega(\xi)) V(x)\, \mathrm{d}\xi\, \mathrm{d}x + E_1(z) \tag{30}$$

where S_z denotes the set of ξ that can be reached (via (29)) for the point z from our survey:

$$S_z = \left\{ \xi = \frac{2\omega}{c_0}(\widehat{\Gamma(s) - z}) : \omega \in \mathrm{eff.supp}(p),\, s \in (s_1^{\min}, s_1^{\max}) \times (s_2^{\min}, s_2^{\max}) \right. \\ \left. \text{and} \quad |\Gamma(s) - z| < c_0 T \right\}. \tag{31}$$

We will see in section 4 that the set S_z determines exactly which singularities in the scattering region can be reconstructed.

Equation (30) exhibits the operator MF as a pseudodifferential operator. Pseudodifferential operators have the *pseudolocal* property [34], i.e. they do not move singularities or change their orientation.

The Jacobian determinant $|\partial(s, \omega)/\partial\xi|$ is also called the *Beylkin determinant* [4, 6]. When $x = z$, its reciprocal is given by

$$\left|\frac{\partial\xi}{\partial(s,\omega)}\right| (z, z, s, \omega) = \frac{8\omega^2}{c_0^3} \frac{1}{|\Gamma(s) - z|^2} \left| P_\perp \frac{\partial\Gamma(s)}{\partial s_1} \quad P_\perp \frac{\partial\Gamma(s)}{\partial s_2} \quad \widehat{\Gamma(s) - z} \right| \tag{32}$$

where $P_\perp = I - (\widehat{\Gamma(s) - z})(\widehat{\Gamma(s) - z})^T$ is the operator that projects a vector onto the plane perpendicular to $\hat{R} = \widehat{\Gamma(s) - z}$. We note that the matrix on the right side of (32) is composed of three vectors, namely (i) $T_1 = P_\perp(\partial\Gamma(s)/\partial s_1)$, (ii) $T_2 = P_\perp(\partial\Gamma(s)/\partial s_2)$ and (iii) $\hat{R}$. Note that T_1 and T_2 are tangent to the unit sphere at $\hat{R}$; see figure 2. These three vectors are clearly independent provided the measurement surface is situated well above z. In this case, the Jacobian determinant (32) is nonzero.

To simplify the notation, we write

$$b(z, x, \xi) = 2\pi A\big(x, s(\xi), |x - \Gamma(s(\xi))|, \omega(\xi)\big) \left|\frac{\partial(s,\omega)}{\partial\xi}\right| (z, x, s(\xi), \omega(\xi)). \tag{33}$$

Remark. We have assumed that the image point z is well below the measurement surface. For such a z, the phase of (26) actually has two critical points, one for which $z = x$ and one for which x is the reflection of z about the measurement surface. However, we assume that this measurement surface is well above the region in which any scatterers are located, so that only the critical point with $z = x$ contributes to (26).

3.2. Amplitude correction

We follow the migration operator M by a post-processing pseudodifferential operator (spatially variable filter) Q that corrects the amplitudes in the image. We choose this operator Q so that QMF looks as much like the identity operator as possible. In particular, the amplitude of QMF should be constant over as large a frequency range as possible. We therefore choose Q to be

$$QI(z) = (2\pi)^{-6} \int e^{i(z-y)\cdot\xi} (b(z, y, \xi))^{-1} \chi(z, y, \xi) I(y)\, d\xi\, dy, \tag{34}$$

where χ is a cutoff function that prevents division by zero in (34). In particular, χ is supported for $z \approx y$ and $\xi \in S_z$, and for points in S_z near its boundary. The composition QMF is thus

$$QMFV(z) = (2\pi)^{-6} \int e^{i(z-y)\cdot\xi} (b(z, y, \xi))^{-1} \chi(z, y, \xi) \times e^{i(y-x)\cdot\tilde{\xi}} b(y, x, \tilde{\xi}) V(x)\, d\tilde{\xi}\, dy\, d\xi\, dx + E_2(z), \tag{35}$$

where again $E_2(z)$ denotes a function smoother than the first term on the right-hand side. In (35) we make the change of variables $\xi \to \rho\xi$ and $\tilde{\xi} \to \rho\tilde{\xi}$, carry out a large-$\rho$ stationary phase reduction in the y and $\tilde{\xi}$ variables, and then revert to the original variables. This results in

$$QMFV(z) = (2\pi)^{-3} \int e^{i(z-x)\cdot\xi} (b(z, x, \xi))^{-1} b(x, x, \xi) \chi(z, x, \xi) V(x)\, d\xi\, dx + E_3(z). \tag{36}$$

3.3. (Asymptotic) inversion

Alternatively, we can apply the migration and amplitude correction steps together in a single asymptotic *inversion* operation by applying the operator

$$(Bd)(z) = (2\pi)^{-4} \int e^{i\omega(t-2|z-\Gamma(s)|/c_0)} (b(z, z, \xi(s, \omega)))^{-1} \chi(z, z, \xi(s, \omega)) d(s, t)\, d\omega\, ds\, dt \tag{37}$$

where we have used the change of variables (29) for ξ. If we substitute $d = FV$ with F given by (18) into (37) and carry out the stationary phase reduction in the t and $\tilde{\omega}$ variables as before, and then change variables from s and ω to ξ, we obtain

$$BFV(z) = \int K(z, x) V(x)\, dx + E_4(z), \tag{38}$$

where

$$K(z, x) = (2\pi)^{-3} \int e^{i(z-x)\cdot\xi} (b(z, z, \xi))^{-1} b(x, z, \xi) \chi(z, z, \xi)\, d\xi \tag{39}$$

is the *point spread function* (i.e. the image due to a delta function point scatterer located at x).

Remark. We can determine the singularities of the functions $QMFV$ and BFV by investigating the large-$|\xi|$ behaviour of (36) and (38) with (39). The leading order behaviour is determined by the kernels at the critical point $z = x$. Since the kernel (39) at $z = x$ is the

same as the kernel of (36) at $z = x$, the operators QMF and BF are the same to leading order, i.e. $QMFV$ and BFV differ only by a smoother function.

Moreover, we note that at the critical point $z = x$, the integrand of (39) is simply a multiple of χ; this shows that to leading order, the point spread function K is an approximate delta function.

The degree to which K approximates a delta function is determined by the support of χ, which is in turn determined though (29) by the extent of the survey and the bandwidth.

4. Resolution

The explicit form of (38) and (39) enables us to determine exactly what information about the scene can be reconstructed. In particular, we can determine the resolution of the imaging system.

By resolution, we mean how far apart two points must be in order for their images to be separated. Specifically, if the image contains Fourier components with magnitude no larger than b, then the resolution is no finer than $2\pi/b$ [28].

To analyse the resolution of (39), we use the simplified notation

$$K(z, x) = \int e^{i(z-x)\cdot\xi} a(z, x, \xi)\, d\xi. \tag{40}$$

We have seen that $a(z, z, \xi)$ is constant over a large region in the variable ξ and is zero outside S_z. The size of this region is determined by the frequency content and the solid angle subtended by the survey.

Equation (40) exhibits the point spread function K as the superposition of frequencies determined by the effective support of $a(z, x, \xi)$ in the ξ variable; the radius of this set is in turn determined by the effective support of p. We see from (5) and (29) that the radius of the support of p is $b = 2\omega_{\max}/c_0$, which implies that a lower bound for the resolution is $2\pi/b = \pi c_0/\omega_{\max}$. If $\lambda_{\min} = 2\pi c_0/\omega_{\max}$ is the wavelength corresponding to $\omega_{\max}$, then the resolution is bounded below by $\pi c_0/\omega_{\max} = \lambda_{\min}/2$.

4.1. Directional resolution

We know from the pseudolocal property of pseudodifferential operators that a singularity at a point z in the image can only come from a singularity in the scene V at the same point. Now suppose that this singularity is associated with a certain direction as in (21).

The operator BF maps a function such as (21) into an image

$$\begin{aligned}\int K(z, x)\delta(x \cdot \hat{v})\, dx &= (2\pi)^{-1} \int K(z, x) e^{ix\cdot\rho\hat{v}}\, d\rho\, dx \\ &= (2\pi)^{-1} \int e^{i(z-x)\cdot\xi} a(z, x, \xi) e^{ix\cdot\rho\hat{v}}\, d\xi\, d\rho\, dx. \end{aligned} \tag{41}$$

In (41) we make the change of variables $\xi \to \rho\tilde{\xi}$, and carry out a large-ρ stationary phase reduction in the variables x and $\tilde{\xi}$. We find, as expected, that the leading order contribution comes from the point $z = x$; the result is

$$\int K(z, x)\delta(x \cdot \hat{v})\, dx = (2\pi)^2 \int a(z, z, \rho\hat{v}) e^{iz\cdot\rho\hat{v}}\, d\rho + E_5(z). \tag{42}$$

We see from (42) that singularities with direction $\hat{v}$ in the scene are carried over to singularities in the image that are also in the direction $\hat{v}$. This is the pseudolocal property

of BF. From (42) we see also that the resolution in direction $\hat{v}$ is determined by the size of the ρ-interval for which $a(z, z, \rho\hat{v})$ is nonzero. Since for $x = z$, we have from (29)

$$\rho\hat{v} = \xi = \frac{2\omega}{c_0}(\widehat{\Gamma(s) - x}), \tag{43}$$

we see that in order for a singularity at the point x with direction $\hat{v}$ to appear in the image, we must include in our survey points on the measurement surface Γ for which $\hat{v} = \widehat{\Gamma(s) - x}$. Moreover, at $\Gamma(s)$, the antenna beam pattern in direction $\widehat{\Gamma(s) - x}$ must be nonzero. If this is the case, then the resolution in the $\hat{v}$ direction is determined by the effective support of p; specifically, we see from (43) that a lower bound for the resolution is $2\pi(2\omega_{\max}/c_0)^{-1} = \pi c_0/\omega_{\max} = \lambda_{\min}/2$.

5. Sampling

The above resolution analysis is based on a continuum model for d. However, in practice, the data are measured as discrete samples, so we must determine how finely the data must be sampled in order for the foregoing analysis to apply. To do this, we calculate the Fourier transform ($\mathcal{F}$) of the data in preparation for using the Shannon sampling theorem [28]:

$$\begin{aligned}\mathcal{F}(d)(\omega, \sigma) &= \int \mathrm{e}^{-\mathrm{i}(\omega t + \sigma\cdot s)} d(t, s)\,\mathrm{d}t\,\mathrm{d}s \\ &= \int \mathrm{e}^{-\mathrm{i}(\omega t+\sigma\cdot s)}\mathrm{e}^{-\mathrm{i}\tilde{\omega}(t-2|z-\Gamma(s)|/c_0)} \cdot A(x, s, t, \tilde{\omega})V(x)\,\mathrm{d}\tilde{\omega}\,\mathrm{d}x\,\mathrm{d}t\,\mathrm{d}s. \end{aligned}\tag{44}$$

For large ω, the leading order contribution to (44) comes from the stationary point where $\tilde{\omega} = \omega$ and

$$\sigma = \frac{2\omega}{c_0}\left(\widehat{x - \Gamma} \cdot \frac{\partial\Gamma}{\partial s_1}, \widehat{x - \Gamma} \cdot \frac{\partial\Gamma}{\partial s_2}\right). \tag{45}$$

From (45) we see that the spatial frequencies that contribute significantly to d are those with magnitude smaller than $b = 2(\omega_{\max}/c_0)$ and the temporal frequencies are those with magnitude smaller than $\omega_{\max}$; the Shannon sampling theorem then tells us that if we sample d with step sizes in s of $\pi/b = \lambda_{\min}/4$ and step sizes in t of $\pi/(\omega_{\max})$, then we can (essentially) recover d for all values of s and t.

6. Example: the CARABAS system

The foliage-penetrating CARABAS II system, described in [18, 23, 40], has $\omega_{\min} = 2\pi \cdot 20 \cdot 10^6$ and $\omega_{\max} = 2\pi \cdot 90 \cdot 10^6$. It uses a two-element phased array of broadband dipole antennas mounted on the front of a Sabreliner aircraft. It typically flies at 100 m s^{-1} at an altitude of 1.5–10 km. Images are produced with a fast backprojection algorithm [26, 38]. Ground topography is found by flying multiple flight tracks several kilometres apart [39].

Our analysis predicts the lower bound for the ideal directional resolution of the single-pass CARABAS system to be $\lambda_{\min}/2 \approx 3.3\ \mathrm{m}/2 \approx 1.6$ m; this is consistent with the analysis of [37]. The performance of the actual system does not quite attain this bound; in [36] this is attributed to the non-ideal nature of the antenna phase response.

Our analysis predicts that the spatial sampling needed to approximate a surface of sensors is about 0.8 m. Using the two antennas of the CARABAS system to approximate a surface, however, is undoubtedly too crude.

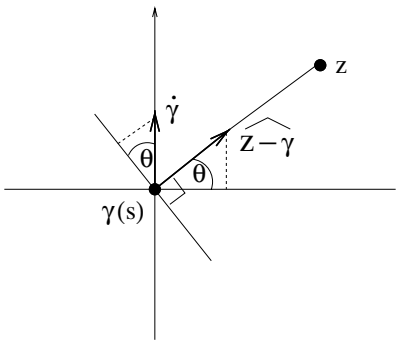

Figure 3. Geometry for single-pass Beylkin determinant.

7. Relation to earlier work

7.1. Imaging from a single flight track

In the case when data is available only from a single pass, microlocal techniques can still be applied. The analysis turns out to be somewhat different, and will be discussed elsewhere, but the methods are closely related to the ones used here. In order to show how our analysis is related to previous work, we give a brief summary here of the results from the single-pass case.

In the case of a single flight pass, the two-dimensional measurement surface Γ is replaced by a single curve $\gamma(s)$, so the data now depends on only two variables (s, t). We can therefore only hope to recover a function of two variables. Accordingly, we assume that the topography is known, and for simplicity, we assume that it is flat. More specifically, we assume that V is given by $V(x) = V(x_1, x_2)\delta(x_3)$, so that the unknown scene is also a function of only two variables. In many cases, this is a reasonable assumption, because electromagnetic waves are rapidly attenuated in the earth, especially if the moisture content is high. It is therefore reasonable to assume that the scattering takes place in a thin region near the surface.

If only a single pass is made, and the antenna has poor directionality, then determining whether a given reflection came from the left or the right of the flight track is problematic [2]. We therefore assume that the antenna is sufficiently directional so that the antenna beam pattern is negligible on one side of the flight path.

Under these assumptions, reconstruction can be done with the same matched filter processing we used in section 3.1. In this case, the Beylkin determinant (32) is the determinant of a two-by-two matrix:

$$\left|\frac{\partial\xi}{\partial(s,\omega)}\right|(z,z,s,\omega) = \frac{4\omega}{c_0^2}\frac{1}{|\gamma(s)-z|}|P_H P_\perp\dot\gamma(s) \quad P_H\widehat{\gamma(s)-z}|, \tag{46}$$

where $\dot\gamma = \mathrm{d}\gamma/\mathrm{d}s$ and P_H denotes the operator which projects onto the horizontal.

If, as in the purely two-dimensional case studied in [1, 16, 22, 26], the flight track is the x_2 axis, then the vectors forming the matrix on the right-hand side of (46) are orthogonal and the second is a unit vector. Therefore the determinant on the right-hand side of (46) is simply the length of the first vector, $|P_\perp\dot\gamma| = \cos\theta$, where θ is the angle formed by the flight track $\dot\gamma$ and the line perpendicular to $\gamma(s) - z$ (see figure 3). Thus the Beylkin determinant is

$$\left|\frac{\partial\xi}{\partial(s,\omega)}\right|(z,z,s,\omega) = \frac{2\xi_1}{c_0|\gamma(s)-z|}, \tag{47}$$

where $\xi_1 = (2\omega/c_0)\cos\theta$. This means that the amplitude correction factor that should be used in (34) and (37) is

$$b(z, z, \xi)^{-1} = \frac{(4\pi)^2|z-\gamma(s)|^2}{2\pi\omega^2 p(\omega) j_s(\omega(\widehat{z-\gamma(s)}), \gamma(s)) j_r(\omega(\widehat{z-\gamma(s)}), \gamma(s)) m(s,t)} \frac{2\xi_1}{c_0|\gamma(s)-z|}. \tag{48}$$

The corresponding filter used in [1, 22, 26] is, in the notation used here, simply $b^{-1}(z, z, \xi) = \xi_1$; this is the same as (48) up to the factors that are ignored in [1, 22, 26], such as $2/c_0$, the antenna beam patterns j_s, j_r, the source signature p, the mute m, and the geometrical spreading factor $|\gamma(s) - z|$.

7.2. Resolution

The approach to resolution that is used in [37] for the single flight-track case is to consider the quotient

$$Q(x) = \frac{\int |K(z,x)|^2 \,\mathrm{d}z}{|K(x,x)|^2}, \tag{49}$$

which is a relative measure of the degree to which information from the point x spreads over the rest of the image.

We analyse Q with the help of expression (40). The numerator of (49) is

$$\int |K(z,x)|^2 \,\mathrm{d}z = \int \mathrm{e}^{\mathrm{i}(z-x)\cdot\xi} a(z,x,\xi) \mathrm{e}^{-\mathrm{i}(z-x)\cdot\eta} \overline{a(z,x,\eta)} \,\mathrm{d}\xi \,\mathrm{d}\eta \,\mathrm{d}z, \tag{50}$$

where the bar denotes complex conjugation. On the right-hand side of (50), we carry out a large-$|\xi|$ stationary phase reduction in the z and η variables. This results in

$$\int |K(z,x)|^2 \,\mathrm{d}z \sim (2\pi)^2 \int a(x,x,\xi)\overline{a(x,x,\xi)} \,\mathrm{d}\xi. \tag{51}$$

The leading order term of the quotient (49) is therefore

$$Q(x) \sim (2\pi)^2 \frac{\int |a(x,x,\xi)|^2 \,\mathrm{d}\xi}{|\int a(x,x,\xi)\,\mathrm{d}\xi|^2}. \tag{52}$$

We obtain an upper bound for the denominator from the Schwarz inequality

$$\left|\int a(x,x,\xi)\,\mathrm{d}\xi\right|^2 \leqslant \int |a(x,x,\xi)|^2 \,\mathrm{d}\xi \int \chi_a(x,\xi)\,\mathrm{d}\xi, \tag{53}$$

where $\chi_a(x,\xi)$ denotes the function that is one on the support of $a(x,x,\xi)$ and zero off it. From (52) we therefore obtain a lower bound for the leading order term of Q:

$$Q(x) \geqslant \frac{(2\pi)^2}{\int \chi_a(x,\xi)\,\mathrm{d}\xi} = \frac{(2\pi)^2}{\int_{S^2}\int_0^\infty \chi_a(x,\rho\hat{v})\rho^2 \,\mathrm{d}\rho \,\mathrm{d}\hat{v}}. \tag{54}$$

This is the same formula as found in [37].

As we see from (33), the volume needed in the denominator of (54) is determined by the mute, i.e. by the bandwidth and the extent of the survey. The corresponding volume in ξ-space is given by the mapping (29). Thus the resolution at a point x is approximately determined by the bandwidth and by the solid angle subtended by the region of the measurement surface from which x is probed.

Acknowledgments

We thank Lars Ulander and his group for discussions and copies of their papers. We are grateful to Eric Todd Quinto for helpful comments on an earlier version of the paper. This work was partially supported by the National Science Foundation through the Engineering Research Centers Program (award number EEC-9986821) and the Focused Research Groups in the Mathematical Sciences Program.

Appendix

In section 3 we need to apply the FIO M to the data d; however, arbitrary FIOs cannot necessarily be applied to any distribution. The data d is in practice band limited and therefore smooth, but as the bandwidth of the system approaches infinity, we need to check that in the limit, Md is well defined.

The condition under which a FIO A can be applied to a distribution v is given in [11], section 2.4; the condition involves the (twisted) *canonical relation* Λ' of the FIO and the *wavefront set* $WF(v)$ of the distribution.

The condition is that $\xi \neq 0$ whenever

$$((x, \xi), (y, \eta)) \in \Lambda' \qquad \text{and} \qquad (y, \eta) \in WF(v). \tag{55}$$

In the case of $A = M$ (22) and $v = d$ (18), the role of y is played by (s, t). From (29), assumption 1, and the assumption that $\omega_{\min}$ is greater than zero, ξ is never zero.

References

[1] Andersson L-E 1988 On the determination of a function from spherical averages *SIAM J. Math. Anal.* **19** 214–32
[2] Agranovsky M and Quinto E T 1996 Injectivity sets for the Radon transform over circles and complete systems of radial functions *J. Funct. Anal.* **139** 383–414
[3] Beylkin G and Burridge R 1990 Linearized inverse scattering problems in acoustics and elasticity *Wave Motion* **12** 15–52
[4] Beylkin G 1985 Imaging of discontinuities in the inverse scattering problem by inversion of a causal generalized Radon transform *J. Math. Phys.* **26** 99–108
[5] Bleistein N and Handelsman R A 1986 *Asymptotic Expansions of Integrals* (New York: Dover)
[6] Bleistein N, Cohen J K and Stockwell J W 2000 *The Mathematics of Multidimensional Seismic Inversion* (New York: Springer)
[7] Cheney M 2001 A mathematical tutorial on Synthetic Aperture Radar *SIAM Rev.* **43** 301–12
[8] Curlander J C and McDonough R N 1991 *Synthetic Aperture Radar* (New York: Wiley)
[9] Carrar W C, Goodman R G and Majewski R M 1995 *Spotlight Synthetic Aperture Radar: Signal Processing Algorithms* (Boston, MA: Artech House Publishers)
[10] Cutrona L J 1990 Synthetic aperture radar *Radar Handbook* 2nd edn, ed M Skolnik (New York: McGraw-Hill)
[11] Duistermaat J J 1996 *Fourier Integral Operators* (Boston: Birkhauser)
[12] Derneryd A and Lagerstedt A 1995 Novel slotted waveguide antenna with polarimetric capabilities *Proc. IGARSS Conf. (Firenze, Italy)* pp 2054–6
[13] Derneryd A G, Petersson R N O and Ingvarson P 1994 Slotted waveguide antennas for remote sensing satellites *Proc. PIERS Conf. (July 1994)* (The Netherlands: Noordwijk)
[14] Edde B 1993 *Radar: Principles, Technology, Applications* (New York: Prentice-Hall)
[15] Elachi C 1987 *Spaceborne Radar Remote Sensing: Applications and Techniques* (New York: IEEE)
[16] Fawcett J A 1985 Inversion of N-dimensional spherical means *SIAM J. Appl. Math.* **45** 336–41
[17] Franceschetti G and Lanari R 1999 *Synthetic Aperture Radar Processing* (New York: CRC Press)
[18] Gustavsson A, Frölind P-O, Hellsten H, Jonsson T, Larsson B, Stenström G and Ulander L M H 1998 Development and operation of the FOA CARABAS HF/VHF-SAR system *Proc. 4th Int. Workshop on Radar Polarimetry (Nantes, France, July 1998)*
[19] Herman G T, Tuy H K, Langenberg K J and Sabatier P C 1988 *Basic Methods of Tomography and Inverse Problems* (Philadelphia, PA: Adam Hilger)

[20] Grigis A and Sjöstrand J 1994 *Microlocal Analysis for Differential Operators: An Introduction (London Mathematical Society Lecture Note Series vol 196)* (Cambridge: Cambridge University Press)
[21] Guillemin V and Sternberg S 1979 *Geometric Asymptotics* (Providence, RI: American Mathematical Society)
[22] Hellsten H and Andersson L E 1987 An inverse method for the processing of synthetic aperture radar data *Inverse Problems* **3** 111–24
[23] Hellsten H, Ulander L M H, Gustavsson A and Larsson B 1996 Development of VHF CARABAS II SAR *SPIE Conf. Proc.* vol 2747 (Bellingham, WA: SPIE Optical Engineering Press) pp 48–60
[24] Langenberg K J, Brandfass M, Mayer K, Kreutter T, Brüll A, Felinger P and Huo D 1993 Principles of microwave imaging and inverse scattering *EARSeL Adv. Remote Sens.* **2** 163–86
[25] Louis A and Quinto E T 2000 Local tomographic methods in SONAR *Surveys on Solution Methods for Inverse Problems* ed D Colton, H W Engl, A K Louis, J R McLaughlin and W Rundell (New York: Springer)
[26] Nilsson S 1997 Application of fast backprojection techniques for some inverse problems of integral geometry *Dissertation* No 499 Linköping Studies in Science and Technology
[27] Nolan C J 2000 Scattering near a fold caustic *SIAM J. Appl. Math.* **61** 659–72
[28] Natterer F 1986 *The Mathematics of Computerized Tomography* (New York: Wiley)
[29] Nolan C J and Symes W W 1997 Global solution of a linearized inverse problem for the acoustic wave equation *Commun. Part. Diff. Eq.* **22**
[30] Oppenheim A V and Shafer R W 1975 *Digital Signal Processing* (Englewood Cliffs, NJ: Prentice-Hall)
[31] Quinto E T 1993 Singularities of the x-ray transform and limited data tomography in R^2 and R^3 *SIAM J. Math. Anal.* **24** 1215–25
[32] Stutzman W L and Thiele G A 1997 *Antenna Theory and Design* (New York: Wiley)
[33] Treves F 1975 *Basic Linear Partial Differential Equations* (New York: Academic)
[34] Treves F 1980 *Introduction to Pseudodifferential and Fourier Integral Operators* vol 1 and 2 (New York: Plenum)
[35] Therrien C W 1992 *Discrete Random Signals and Statistical Signal Processing* (Englewood Cliffs, NJ: Prentice-Hall)
[36] Ulander L M H 1998 Approaching the wavelength resolution limit in ultra-wideband VHF-SAR *Proc. PIERS Workshop on Advances in Radar Methods (Beveno, Italy, July 1998) Report EUR* 18662 EN Space Applications Institute, Joint Research Centre of the European Commission
[37] Ulander L M H and Hellsten H 1996 A new formula for SAR spatial resolution *AEÜ Int. J. Electron. Commun.* **50** 117–21
[38] Ulander L M H, Hellsten H and Stenström G 2000 Synthetic-aperture radar processing using fast factorised backprojection *Preprint*
[39] Ulander L M H and Frölund P-O 1998 Ultra-wideband SAR interferometry *IEEE Trans. Geosci. Remote Sens.* **36** 1540–50
[40] Ulander L M H and Hellsten H 1999 Low-frequency ultra-wideband array-antenna SAR for stationary and moving target imaging *Conf. Proc. SPIE 13th Annual Int. Symp. on Aerosense (Orlando, FL, April 1999)*
[41] Ziomek L J 1985 *Underwater Acoustics: A Linear Systems Theory Approach* (Orlando, FL: Academic)
[42] Zahn R and Schlott M 1994 Active antenna for X-band space SAR *Proc. Int. Conf. on Radar (Paris, France)* pp 36–41